

Study of forbidden β decays within the realistic shell model

G. De Gregorio,^{1,2} R. Mancino,^{3,4,5} L. Coraggio,^{1,2} and N. Itaco^{1,2}

¹*Dipartimento di Matematica e Fisica, Università degli Studi della Campania “Luigi Vanvitelli”,
viale Abramo Lincoln 5 - I-81100 Caserta, Italy*

²*Istituto Nazionale di Fisica Nucleare,
Complesso Universitario di Monte S. Angelo, Via Cintia - I-80126 Napoli, Italy*

³*Institute of Particle and Nuclear Physics, Faculty of Mathematics and Physics,
Charles University, V Holešovičkách 2, 180 00 Prague, Czech Republic*

⁴*Institut für Kernphysik (Theoriezentrum), Fachbereich Physik, Technische Universität Darmstadt,
Schlossgartenstrasse 2 - 64298 Darmstadt, Germany*

⁵*GSI Helmholtzzentrum für Schwerionenforschung, Planckstrasse 1, 64291 Darmstadt, Germany*

For the first time, half-lives and energy spectra of forbidden β decays are calculated within the realistic shell model. Namely, we approach this issue starting from a realistic nucleon-nucleon potential and deriving effective Hamiltonians and decay operators. Our goal is to explore the sensitivity of the shape of calculated energy spectra to the renormalization of forbidden β -decay operators, an operation that allows to take into account those configurations that are not explicitly included in the chosen model space. The region that has been considered for this investigation are nuclei outside the ^{78}Ni core, more precisely we have studied the second-forbidden β decays of ^{94}Nb and ^{99}Tc , and fourth-forbidden β decays of ^{113}Cd and ^{115}In , that are currently of a renewed experimental interest in terms of novel spectroscopic techniques. Our results evidence that the introduction of a renormalized β -decay operator leads to a marked improvement of the reproduction of experimental half-lives. As regards the spectra of both second-forbidden and fourth-forbidden decays, we have found that their calculated shapes are in good agreement with the observed ones, even if scarcely responsive to the renormalization of the decay operator. We carry out also a detailed inspection of the different components of the calculated spectra for a deeper insight about their role in reproducing the experimental shapes.

PACS numbers: 21.60.Cs, 21.30.Fe, 27.60.+j

I. INTRODUCTION

The understanding of the renormalization mechanisms of electroweak currents is nowadays a cornerstone of the nuclear structure research. The attention to this issue is motivated by the need of calculating reliable nuclear matrix elements $M^{0\nu}$ for the $0\nu\beta\beta$ decay, and relating the inverse half-life $[T_{1/2}^{0\nu}]^{-1}$ of such a rare process to the neutrino effective mass.

As a matter of fact, the accurate calculation of the wave functions of parent and grand-daughter nuclei does not ensure a trustable $M^{0\nu}$, since most nuclear models are based on the reduction of the dimension of the Hilbert space where the nuclear Hamiltonian is defined. Then, a sound knowledge of the renormalization of the electroweak currents, to account for the configurations that are not explicitly included in the components of the nuclear wave function, is crucial to enhance the predictivity of the calculated $M^{0\nu}$ s.

The ability of nuclear models to reproduce β -decay observables is, consequently, the better way to validate both wave functions and renormalization procedures, and such an issue is connected to the so-called “quenching puzzle” of the axial coupling constant, namely the need by most nuclear structure models to resort to a reduction of g_A to reproduce the observables directly linked to Gamow-Teller (GT) transitions [1–3]. However, this is an empirical procedure, and it cannot be generalized to any

β -decay operator that depends on the value of the axial coupling constant.

The realistic shell model (RSM) provides a consistent approach to derive effective Hamiltonians and decay operators, the only parameter that is involved being the nuclear force one starts from. In such a framework, single-particle (SP) energies and two-body matrix elements (TBMEs) of the effective shell-model Hamiltonian H_{eff} , as well as every matrix element of decay operators, are derived from a realistic free nucleon-nucleon (NN) potential V_{NN} by way of the many-body theory [4, 5]. The bare matrix elements of the NN potential, and of any transition operator, are renormalized with respect to the truncation of the full Hilbert space into the reduced shell-model (SM) model space, to take into account the neglected degrees of freedom without resorting to any empirical parameter [6]. In other words, this approach does not apply effective charges to calculate electromagnetic transition strengths, and empirical quenching of g_A to reproduce the β -decay matrix elements.

We have successfully employed RSM to study the $2\nu\beta\beta$ -decay of ^{48}Ca , ^{76}Ge , ^{82}Se , ^{100}Mo , ^{130}Te , and ^{136}Xe [7–10], and then extended it to predict the nuclear matrix elements of their $0\nu\beta\beta$ -decay [9, 11]. Now, in order to validate the RSM in predicting β -decay observables, in the present work we investigate the sensitivity to the renormalization of SM forbidden β -decay operators describing the energy spectra of the emitted electrons.

To this end, we have considered the second-forbidden

β -decays of ^{94}Nb and ^{99}Tc into ^{94}Mo and ^{99}Ru , as well as the fourth-forbidden β -decays of ^{113}Cd and ^{115}In into ^{113}In and ^{115}Sn , respectively, and compared their calculated $\log fts$ and β -decay energy spectra as obtained with the bare and the renormalized decay operators, as well as with the available data.

The motivations of such a choice are twofold: first, these decays have been already the subject of a few works with a similar goal, where the effective operators was obtained tuning the quenching factor q of g_A , and the focus was spotted on the dependence of the shape of energy spectra on the value of q [12–16]. Second, novel experimental techniques have triggered new measurements of the energy spectra of β decays in the region of the $0\nu\beta\beta$ decay of ^{100}Mo . Among them, we mention the COBRA demonstrator [17], that has been developed for double- β decay experiments, and also adopted to study the spectra of β decays of ^{113}Cd [15, 18, 19]; the ACCESS project that aims to perform precision measurements of forbidden β -decays using cryogenic calorimeters [20]. Another new experimental project is ASPECT-BET (An SDD-SPECTrometer for BETA decay studies), that has developed a new detection strategy based on silicon drift detectors (SDD), and it should be able to perform high-precision, high-accuracy measurements of the energy spectra of β decays at room temperature [21].

This paper is organized as follows. First, in Sec. II we sketch out briefly the derivation of the effective SM Hamiltonian and decay operators, as well as the basic theory of the β -decay and the structure of the second- and fourth-forbidden β -decay matrix elements.

The effective shell-model Hamiltonian and decay operators have been derived within a model space that is spanned by four $0f_{5/2}, 1p_{3/2}, 1p_{1/2}, 0g_{9/2}$ proton orbitals and five $0g_{7/2}, 1d_{5/2}, 1d_{3/2}, 2s_{1/2}, 0h_{11/2}$ neutron orbitals outside ^{78}Ni core starting from the high-precision CD-Bonn NN potential [22], whose repulsive high-momentum components are renormalized using the $V_{\text{low-}k}$ procedure [23]. This is the same framework we have employed in our previous study of the double- β decay of ^{100}Mo [9].

The results of the shell-model calculations are discussed and compared with the available experimental data in Sec. III. There, we check first our nuclear wave functions by comparing the calculated low-energy spectra and $E2$ transition strengths of parent and daughter nuclei, which are involved in the decays under consideration, with their experimental counterparts. Then, we report the results of our theoretical $\log fts$ and energy spectra of the emitted electron and size up them to the available data. We complete our analysis with a detailed analysis of the different components of the spectra, and how the interplay among their contributions plays an important role in reproducing data.

In the last section (Sec. IV), we summarize the conclusions of this study, as well as the outlook of our current research project.

II. OUTLINE OF THE THEORY

A. The effective SM Hamiltonian

The procedure of the derivation of the effective SM Hamiltonian is the same as the one followed in Ref. [9]. First, we consider the high-precision CD-Bonn NN potential [22], then the non-perturbative repulsive high-momentum components are integrated out, by way of the $V_{\text{low-}k}$ unitary transformation [23, 24], that provides a smooth potential preserving all the two-nucleon observables calculated with the CD-Bonn one.

The $V_{\text{low-}k}$ matrix elements are chosen as the interaction vertices of a perturbative expansion of H_{eff} , as well as those of the Coulomb interaction between protons, and a detailed description of the many-body perturbation theory approach to the nuclear H_{eff} can be found in Refs. [6, 25, 26], so here we only sketch briefly the steps that have been followed to obtain H_{eff} .

The starting point is the full nuclear Hamiltonian H for A interacting nucleons, which, according to the SM ansatz, is divided into the one-body term H_0 , whose eigenvectors set up the SM basis, and the residual interaction H_1 , using the harmonic-oscillator (HO) auxiliary potential U :

$$\begin{aligned} H &= T + V_{\text{low-}k} = (T + U) + (V_{\text{low-}k} - U) = \\ &= H_0 + H_1 . \end{aligned} \quad (1)$$

The eigenvalue problem of H for a many-body system, in an infinite basis of eigenvectors of H_0 , cannot be solved, then an effective Hamiltonian is derived, which is defined in the truncated model space spanned by four proton $- 0f_{5/2}, 1p_{3/2}, 1p_{1/2}, 0g_{9/2}$ – and five neutron orbitals $- 0g_{7/2}, 1d_{5/2}, 1d_{3/2}, 2s_{1/2}, 0h_{11/2}$ – outside ^{78}Ni core.

The effective Hamiltonian is derived by way of the time-dependent perturbation theory, through the Kuo-Lee-Ratcliff folded-diagram expansion in terms of the \hat{Q} -box vertex function [4, 25, 26]:

$$H_1^{\text{eff}}(\omega) = \hat{Q}(\epsilon_0) - PH_1Q \frac{1}{\epsilon_0 - QHQ} \omega H_1^{\text{eff}}(\omega) , \quad (2)$$

where ω is the wave operator decoupling the model space P and its complement Q , and ϵ_0 is the eigenvalue of the unperturbed degenerate Hamiltonian H_0 .

The \hat{Q} box is defined as

$$\hat{Q}(\epsilon) = PH_1P + PH_1Q \frac{1}{\epsilon - QHQ} QH_1P , \quad (3)$$

and ϵ is an energy parameter called “starting energy”.

Since the exact calculation of the \hat{Q} box is not possible, then the term $1/(\epsilon - QHQ)$ is expanded as a power series

$$\frac{1}{\epsilon - QHQ} = \sum_{n=0}^{\infty} \frac{1}{\epsilon - QH_0Q} \left(\frac{QH_1Q}{\epsilon - QH_0Q} \right)^n , \quad (4)$$

namely we perform an expansion of the \hat{Q} box up to the third order in perturbation theory [6].

We would point out that, as in previous works [7–9, 11], we include a number of intermediate states in the perturbative expansion of the shell-model effective Hamiltonian and decay operators, whose maximum allowed excitation energy – expressed in terms of the number of oscillator quanta N_{\max} [26] – is $N_{\max}=16$. This set of intermediate states is sufficient to obtain convergent values of the single-particle energies, TBMEs, and matrix elements of the decay operators, as it has been shown in Refs. [11, 27].

As a matter of fact, the calculation of the \hat{Q} box is the start to solve the non-linear matrix equation (2) and obtain H_{eff} by way of iterative techniques such as the Kuo-Krenciglowa and Lee-Suzuki ones [28, 29], or graphical non-iterative methods [30].

It should be pointed out that, since the nuclei that are involved in the decay processes under investigation are characterized by a large number of valence nucleons, we have included contributions from induced three-body forces in the calculation of the \hat{Q} box, that involve also three valence nucleons.

Since the SM code we have employed for our calculations [31] cannot diagonalize a three-body H_{eff} , we have performed a normal-ordering decomposition of the three-body induced-force contributions arising at second order in perturbation theory, and retained only the two-body term that is density-dependent from the number of valence nucleons. This procedure is presented in details in Refs. [6, 32], together with a discussion about the contribution of such terms to the eigenvalues of the SM Hamiltonian.

The SM parameters, namely the SP energies and the TBMEs of the residual interaction, are reported in the Supplemental Material [33].

B. β -decay theory

The theory of β -decay is here briefly outlined. More details can be found in Refs. [34, 35].

In the following we focus on the β^- -decay, moreover, we use natural units ($\hbar = c = m_e = 1$).

The total half-life of the β decay is expressed in terms of the k -th partial decay half-life $t_{1/2}^k$ as follows:

$$\frac{1}{T_{1/2}} = \sum_k \frac{1}{t_{1/2}^k}. \quad (5)$$

On the other hand, the partial half-life $t_{1/2}^k$ is related to the dimensionless integrated shape function \tilde{C} by way of the relation:

$$t_{1/2}^k = \frac{\kappa}{\tilde{C}}, \quad (6)$$

where $\kappa = 6144 \pm 2$ s [36].

For a given k -th final state, the integrated shape function \tilde{C} – whose integrand defines the β -decay energy spectrum – is written as

$$\tilde{C} = \int_1^{w_0} C(w_e) p_e w_e (w_0 - w_e)^2 F(Z, w_e) dw_e. \quad (7)$$

The quantities on the right-hand side of the above definition are listed as:

- a) Z is the atomic number of the daughter nucleus, w_e the adimensional energy of the emitted electron, w_0 the endpoint energy – namely the maximum electron energy for a given transition –, and p_e the electron momentum.
- b) The function $F(Z, w_e)$ is the Fermi function which is factorized in terms of two functions F_0 and L_0 :

$$F(Z, w_e) = F_0(Z, w_e) L_0(Z, w_e), \quad (8)$$

where F_0 defines the effects of the Coulomb interaction between the electron and the daughter nucleus, and L_0 accounts for the electromagnetic finite-size effect, whose explicit expressions can be found in Ref. [34].

- c) $C(w_e)$ is the so-called nuclear shape function, which depends on the nuclear matrix elements (NMEs). For allowed β transitions, it corresponds to the GT reduced transition probability, and in such a case does not depend on the electron energy.

For n -forbidden transitions, $C(w_e)$ depends on the electron energy, and is expressed as

$$C(w_e) = \sum_K \sum_{k_e, k_\nu} \lambda_{k_e} \left[M_K^2(k_e, k_\nu) + m_K^2(k_e, k_\nu) - \frac{2\gamma_{k_e}}{k_e w_e} M_K(k_e, k_\nu) m_K(k_e, k_\nu) \right], \quad (9)$$

where K is the tensor rank of the forbidden β -decay operators involved in the decay. K can range from 0 to 2 for $n = 1$, and from n to $n + 1$ for $n > 1$. The quantities k_e and k_ν are the positive integers emerging from the partial wave expansion of the leptonic wave functions. The latter, for a given value of K , must satisfy either $k_e + k_\nu = K + 1$ or $k_e + k_\nu = K + 2$.

The auxiliary quantities γ_{k_e} and λ_{k_e} are defined as

$$\gamma_{k_e} = \sqrt{k_e^2 - (\alpha Z)^2}, \quad \lambda_{k_e} = \frac{F_{k_e-1}(Z, w_e)}{F_0(Z, w_e)}, \quad (10)$$

where $F_{k_e-1}(Z, w_e)$ is the so-called generalized Fermi function (see Ref. [34] for its explicit expression). The quantities M_K and m_K are complicated combinations of some kinematic factors and coefficients $F_{KLS}^{(N)}(k_e, m, n, \rho)$, the latter being functions of the orbital, spin, and total rank of the transition operators L , S , and K , respectively, and the integers m , n and

ρ depending on the nuclear charge distribution which accounts for the influence of the nuclear charge on the electron [34, 35]. The index N labels the order of the expansion in powers of qR (where R is the nuclear radius and q is the momentum transfer $q = |p_e + p_\nu|$) of the nuclear form factor F_{KLS} , which is defined by the following expression

$$F_{KLS}(q^2) = \sum_N \frac{(-1)^N (qR)^{2N} (2L+1)!!}{(2N)!! (2L+2N+1)!!} F_{KLS}^{(N)}. \quad (11)$$

If we adopt the impulse approximation ($qR \ll 1$) to derive the formalism of forbidden β -decay transitions, and also assume that bound nucleons interact weakly as free nucleons, then we may neglect the effect of any many-body current. Within such an approximation, it has

$${}^{V/A}M_{KLS}^{(N)}(k_e, m, n, \rho) = \frac{1}{\hat{J}_i} \sum_{\pi, \nu} {}^{V/A}m_{KLS}^{(N)}(\pi, \nu)(k_e, m, n, \rho) \times \text{OBTD}(\Psi_f, \Psi_i, \pi, \nu, K), \quad (13)$$

where $\hat{J}_i = \sqrt{2J_i + 1}$, and J_i is the angular momentum of the initial state of the parent nucleus. The OBTDs are defined as

$$\text{OBTD}(\Psi_f, \Psi_i, \pi, \nu, K) = \frac{\langle \Psi_f || [a_\pi^\dagger \otimes \tilde{a}_\nu]^K || \Psi_i \rangle}{\hat{K}}, \quad (14)$$

where Ψ_i and Ψ_f are the wave function of the initial and

been shown in Refs. [34, 35] that the form factor coefficients ${}^{V/A}F_{KLS}^{(N)}(k_e, m, n, \rho)$ can be related to the NMEs ${}^{V/A}M_{KLS}^N(k_e, m, n, \rho)$ by a phase factor:

$${}^{V/A}F_{KLS}^{(N)}(k_e, m, n, \rho) = (-1)^{K-L} {}^{V/A}M_{KLS}^N(k_e, m, n, \rho), \quad (12)$$

where the label V/A indicates the separation of the coefficients $F_{KLS}^{(N)}(k_e, m, n, \rho)$ according to the axial and vector components of the decay operator.

In a shell-model calculation, the NMEs can be expressed in terms of the single-particle matrix elements of the one-body decay operator (SPMEs) and the one-body transition densities (OBTDs), that can be obtained from the shell-model wave functions, through the expression

final state, respectively, a_π^\dagger is the particle creation operator, and $\tilde{a}_\nu = (-1)^{j_\nu + m_\nu} a_{\nu - m_\nu}$ is the tensor spherical form of the particle annihilation operator (a_ν). The indices π and ν label the proton (π) and neutron (ν) single-particle states, and the symbol \otimes denotes the angular-momentum coupling.

The SPMEs correspond to the following matrix elements:

$${}^V m_{KLS}^{(N)}(k_e, m, n, \rho) = \langle \phi_{\kappa\pi\mu} || \left(\frac{r}{R}\right)^{L+2N} \mathcal{I}(k_e, m, n, \rho, r) T_{KLS} || \phi_{\kappa\nu\mu} \rangle, \quad (15)$$

$${}^A m_{KLS}^{(N)}(k_e, m, n, \rho) = \langle \phi_{\kappa\pi\mu} || \left(\frac{r}{R}\right)^{L+2N} \mathcal{I}(k_e, m, n, \rho, r) \gamma_5 T_{KLS} || \phi_{\kappa\nu\mu} \rangle. \quad (16)$$

Now, it is worth to list and specify the quantities which appear in the Eqs. (15,16) for the matrix elements of the vector and axial components of the β -decay operator:

- The functions $\mathcal{I}(k_e, m, n, \rho, r)$ are the so-called Coulomb factors whose explicit expression can be found in Ref. [34].
- The operator T_{KLS} is the transition operator defined as

$$T_{KLS}^M = \begin{cases} Y_{LM} \delta_{KL} & S = 0, \\ (-1)^{L-K+1} \gamma_5 [Y_L \otimes \sigma]_{KM} & S = 1. \end{cases} \quad (17)$$

- The single-particle relativistic wave functions $\phi_{\kappa\mu}$ are the eigenfunctions of the operators J_z and $\mathcal{K} = \beta(\sigma \cdot L + \mathbb{I})$, and are labeled by their eigenvalues μ

and κ :

$$\begin{aligned} J_z \phi_{\kappa\mu} &= \mu \phi_{\kappa\mu}, \\ \mathcal{K} \phi_{\kappa\mu} &= \beta(\sigma \cdot L + \mathbb{I}) \phi_{\kappa\mu} = \kappa \phi_{\kappa\mu}. \end{aligned}$$

It can be shown that the eigenvalue κ is related to the total and orbital angular momenta j and l through the relation

$$\kappa = \begin{cases} j + \frac{1}{2} & \text{for } l = j + \frac{1}{2} \\ -(j + \frac{1}{2}) & \text{for } l = j - \frac{1}{2}. \end{cases} \quad (18)$$

In the Condon-Shortley (CS) phase convention, the $\phi_{\kappa\mu}$ functions are defined as

$$\phi_{\kappa\mu} = \begin{pmatrix} -i f_\kappa(r) \chi_{-\kappa\mu} \\ g_\kappa(r) \chi_{\kappa\mu} \end{pmatrix}, \quad (19)$$

where $\chi_{\kappa\mu} = [Y_l(\hat{r}) \otimes \chi]^{j\mu}$, and the radial functions $f_\kappa(r)$ and $g_\kappa(r)$ are the solutions of the radial Dirac equations, and they are usually indicated as the *small* and *large* components, respectively:

$$\frac{dg_\kappa(r)}{dr} + \frac{\kappa + 1}{r}g_\kappa(r) - (E + M - V(r))f_\kappa(r) = 0, \quad (20)$$

$$\frac{df_\kappa(r)}{dr} - \frac{\kappa - 1}{r}f_\kappa(r) + (E - M - V(r))g_\kappa(r) = 0. \quad (21)$$

The matrix elements of Eqs. (15,16) can be grouped

$$\begin{aligned} V m_{KK0}^{(N)}(\pi, \nu)(k_e, m, n, \rho) = \sqrt{2}g_V \left[G_{KK0}(\kappa_\pi, \kappa_\nu) \int_0^\infty g_\pi(r, \kappa_p) \left(\frac{r}{R}\right)^{K+2N} \mathcal{I}(k_e, m, n, \rho, r) g_\nu(r, \kappa_\nu) r^2 dr \right. \\ \left. + G_{KK0}(-\kappa_\pi, -\kappa_\nu) \int_0^\infty f_\pi(r, \kappa_\pi) \left(\frac{r}{R}\right)^{K+2N} \mathcal{I}(k_e, m, n, \rho, r) f_\nu(r, \kappa_\nu) r^2 dr \right], \quad (22) \end{aligned}$$

$$\begin{aligned} A m_{KL1}^{(N)}(\pi, \nu)(k_e, m, n, \rho) = \text{sign}(K - L + \frac{1}{2}) \sqrt{2}g_A \left[G_{KK0}(\kappa_\pi, \kappa_\nu) \int_0^\infty g_\pi(r, \kappa_\pi) \left(\frac{r}{R}\right)^{L+2N} \mathcal{I}(k_e, m, n, \rho, r) g_\nu(r, \kappa_\nu) r^2 dr \right. \\ \left. + G_{KK0}(-\kappa_\pi, -\kappa_\nu) \int_0^\infty f_\pi(r, \kappa_p) \left(\frac{r}{R}\right)^{L+2N} \mathcal{I}(k_e, m, n, \rho, r) f_\nu(r, \kappa_\nu) r^2 dr \right]. \quad (23) \end{aligned}$$

The second group contains the product of the small and large components of the initial and final wave func-

into two different types.

The first one contains the product of both small components of the initial and final wave functions, as well as the product of both large components of the same wave functions, which are the solutions of the coupled equations (20,21), and usually they are dubbed in literature as the *non-relativistic* matrix elements [34, 35, 37, 38]. Their explicit expression is:

tions that are the solutions of Eqs. (20,21), and in such a case they are dubbed as the *relativistic* matrix elements. Now, their expression is:

$$\begin{aligned} V m_{KL1}^{(N)}(\pi, \nu)(k_e, m, n, \rho) = \text{sign}(K - L + \frac{1}{2}) \sqrt{2}g_V \left[G_{KL1}(\kappa_\pi, -\kappa_\nu) \int_0^\infty g_\pi(r, \kappa_\pi) \left(\frac{r}{R}\right)^{L+2N} \mathcal{I}(k_e, m, n, \rho, r) f_\nu(r, \kappa_\nu) r^2 dr \right. \\ \left. - G_{KK0}(-\kappa_\pi, \kappa_\nu) \int_0^\infty f_\pi(r, \kappa_\pi) \left(\frac{r}{R}\right)^{L+2N} \mathcal{I}(k_e, m, n, \rho, r) g_\nu(r, \kappa_\nu) r^2 dr \right], \quad (24) \end{aligned}$$

$$\begin{aligned} A m_{KK0}^{(N)}(\pi, \nu)(k_e, m, n, \rho) = \sqrt{2}g_A \left[G_{KK0}(\kappa_\pi, -\kappa_\nu) \int_0^\infty g_\pi(r, \kappa_\pi) \left(\frac{r}{R}\right)^{K+2N} \mathcal{I}(k_e, m, n, \rho, r) f_\nu(r, \kappa_\nu) r^2 dr \right. \\ \left. - G_{KK0}(-\kappa_\pi, \kappa_\nu) \int_0^\infty f_\pi(r, \kappa_\pi) \left(\frac{r}{R}\right)^{K+2N} \mathcal{I}(k_e, m, n, \rho, r) g_\nu(r, \kappa_\nu) r^2 dr \right]. \quad (25) \end{aligned}$$

It is worth to note that in the above equations we have introduced the quantity

$$G_{KLS}(\kappa_\pi, \kappa_\nu) = (-1)^{j_\pi - j_\nu + l_\pi} \hat{S} \hat{K} \hat{j}_\pi \hat{j}_\nu \hat{l}_\pi \hat{l}_\nu \langle l_\pi l_\nu 00 | L0 \rangle \times \begin{Bmatrix} K & S & L \\ j_\pi & \frac{1}{2} & l_\pi \\ j_\nu & \frac{1}{2} & l_\nu \end{Bmatrix}, \quad (26)$$

and we remind that L , S , and K are the orbital, spin, and total rank of the transition operators, respectively, and $l_\tau = k_\tau$ if $k_\tau > 0$ and $l_\tau = |k_\tau| - 1$ if $k_\tau < 0$.

Until now, the nucleon wave functions are expressed in a fully relativistic framework, being the solutions of the Dirac equation. However, within the nuclear shell model, the nucleon wave functions are expressed as solutions of

the single-particle Schrödinger equation, introducing the auxiliary harmonic-oscillator potential.

Such an inconsistency impacts especially on the calculation of the *relativistic* matrix elements, and this problem may be tackled in two ways. The first approach is to resort to a non-relativistic reduction of the Dirac equation by considering the non-relativistic limit of the coupled Eqs. (20,21), namely the kinetic energy T and the auxiliary potential $V(r)$ satisfy the conditions $T = E - M_N \ll 2M_N$ and $V(r) \ll 2M_N$ [39]. Within this limit, the function g_κ becomes the solution of the Schrödinger equation, and f_κ is related to g_κ through the relation

$$f_\kappa(r) = \frac{1}{2M_N} \left(\frac{d}{dr} + \frac{\kappa + 1}{r} \right) g_\kappa(r). \quad (27)$$

However, as it was observed in Ref. [34], whether or not such a limit of the Dirac equation is a good approximation to calculate the *relativistic* NMEs is a difficult question to answer, since to test this approach a fully relativistic calculation should be performed and compared with the approximated results.

Moreover, it should be noted that, if we consider the relation (27), the radial function $f_\kappa(r)$ is suppressed by a factor $1/(2M_N)$ with respect to the function $g_\kappa(r)$, but the *relativistic* form factor, even if it is small with respect to the *non-relativistic* ones, it has been found to be relevant to determine both the shape of the energy spectrum and the half-life of the β decay [35, 37, 40–42].

Its relevance, within such a reduction of the Dirac equation, is also stressed in Ref. [15], where a study of the dependence of the energy spectrum and half-life of the fourth-forbidden β decay of ^{113}Cd with respect to the quenching factor q of the axial coupling constant g_A has been carried out. As a matter of fact, the authors show that a fitting procedure of both q and of the *relativistic* form factor is needed to reproduce the experimental shape of the energy spectrum as well as the observed half-life.

An alternative approach to calculate the *relativistic* NMEs, is to resort to the conserved vector current theory (CVC) [34], which leads to derive a connection between the *relativistic* NMEs and the *non-relativistic* ones, that is developed as a relation between the corresponding form factors. An early application of this approach can be found in Ref. [37].

In particular, for the four decays under investigation, since we stop at the leading order in the expansion of $F_{KLS}(q^2)$ ($N = 0$ in Eq. (11)), the *relativistic* form factors entering in Eq. (9) are only the ${}^V F_{211}$, for the second-forbidden decay of ^{94}Nb , ^{99}Tc , and the ${}^V F_{431}$ for the fourth-forbidden decay of ^{113}Cd , ^{115}In . These form factors, using the CVC relation [34, 37], depend on ${}^V F_{220}$ and ${}^V F_{440}$, respectively, through the relations

$${}^V F_{211} = -\frac{1}{\sqrt{10}} R E_\gamma {}^V F_{220}, \quad {}^V F_{431} = -\frac{1}{\sqrt{36}} R E_\gamma {}^V F_{440}, \quad (28)$$

where

$$E_\gamma = [W_0 + \Delta E_C - (M_\nu - M_\pi)], \quad (29)$$

is the energy of the analogue electromagnetic transition [43], $M_{\nu(\pi)}$ is the neutron (proton) mass, and ΔE_C is the Coulomb displacement energy that can be evaluated in different ways. ΔE_C can be evaluated in different ways, here we have used the results of the fit procedure as outlined in Ref. [44], obtaining $\Delta E_C = 11.99, 12.38, 13.27$, and 13.48 MeV for ^{94}Nb , ^{99}Tc , ^{113}Cd , and ^{115}In decays, respectively.

It is important to stress that these CVC relations have been employed in different studies, leading to a general improvement of the calculated spectra [35, 37, 40–42] and half-lives.

However, we point out that these relations are valid in the full nuclear Hilbert space of the single-particle configurations, and it is difficult to evaluate the impact of resorting to a truncated model space, but, on the other hand, it should be noted that our approach relies on the derivation of effective Hamiltonians and operators by way of the many-body theory to account for the configurations outside the model space.

Nevertheless, the CVC relations for the relativistic form factors represent a viable route to get an estimation of the *relativistic* matrix elements entering the calculation, and/or, to understand the reliability of the non-relativistic reduction of the *relativistic* matrix elements.

C. Effective shell-model decay operators

In this section, we sketch briefly the procedure to derive effective SM decay operators Θ_{eff} by way of many-body perturbation theory.

As is well known, the diagonalization of the H_{eff} does not produce the true nuclear wave-functions, but their projections onto the chosen model space P . Then, any decay operator Θ should be renormalized by taking into account for the neglected degrees of freedom corresponding to the Q subspace.

The derivation of effective SM operators within a perturbative approach traces back to the pioneering period of employing NN potentials in SM calculations [45–50]. We have followed the method that has been introduced by Suzuki and Okamoto [5], which allows a derivation of decay operators Θ_{eff} which is consistent with the one of H_{eff} , as presented in Sec. II A. This is based on the perturbative expansion of a vertex function $\hat{\Theta}$ box – analogously with the derivation of H_{eff} in terms of the \hat{Q} box –, whose details may be found in Refs. [5, 6].

According to such a procedure, the starting point is the perturbative calculation of two energy-dependent vertex functions:

$$\hat{\Theta}(\epsilon) = P\Theta P + P\Theta Q \frac{1}{\epsilon - QHQ} QH_1 P,$$

$$\hat{\Theta}(\epsilon_1; \epsilon_2) = PH_1 Q \frac{1}{\epsilon_1 - QHQ} Q\Theta Q \frac{1}{\epsilon_2 - QHQ} QH_1 P,$$

and of their derivatives calculated in $\epsilon = \epsilon_0$, ϵ_0 being the eigenvalue of the degenerate unperturbed Hamiltonian H_0 :

$$\hat{\Theta}_m = \frac{1}{m!} \left. \frac{d^m \hat{\Theta}(\epsilon)}{d\epsilon^m} \right|_{\epsilon=\epsilon_0},$$

$$\hat{\Theta}_{mn} = \frac{1}{m!n!} \left. \frac{d^m}{d\epsilon_1^m} \frac{d^n}{d\epsilon_2^n} \hat{\Theta}(\epsilon_1; \epsilon_2) \right|_{\epsilon_1=\epsilon_0, \epsilon_2=\epsilon_0}$$

Then, a series of operators χ_n is calculated:

$$\begin{aligned}\chi_0 &= (\hat{\Theta}_0 + h.c.) + \hat{\Theta}_{00} , \\ \chi_1 &= (\hat{\Theta}_1 \hat{Q} + h.c.) + (\hat{\Theta}_{01} \hat{Q} + h.c.) , \\ \chi_2 &= (\hat{\Theta}_1 \hat{Q}_1 \hat{Q} + h.c.) + (\hat{\Theta}_2 \hat{Q} \hat{Q} + h.c.) + \\ &\quad (\hat{\Theta}_{02} \hat{Q} \hat{Q} + h.c.) + \hat{Q} \hat{\Theta}_{11} \hat{Q} . \\ &\dots\end{aligned}\quad (30)$$

At the end, Θ_{eff} is written in the following form:

$$\Theta_{\text{eff}} = H_{\text{eff}} \hat{Q}^{-1} (\chi_0 + \chi_1 + \chi_2 + \dots) , \quad (32)$$

the χ_n series being arrested in our calculations at $n = 2$, and the $\hat{\Theta}$ function expanded up to third order in perturbation theory.

In Refs. [8, 11, 27] we have tackled the issue of the convergence of the χ_n series and of the perturbative expansion of the $\hat{\Theta}$ box, showing the robustness of such a procedure.

It is worth to point out that, even if the decay operator has a one-body structure, the shell-model effective operator has many-body components which account for a number of valence of nucleons larger than one [11, 48]. As a matter of fact, the fourth-forbidden β decay of ^{115}In into ^{115}Sn involves 37 valence nucleons outside the doubly-magic ^{78}Ni , then for such a process Θ_{eff} should contain contributions up to a 37-body term.

The shell-model code KSHELL can employ transition operators with a one- and two-body components [31], then for the calculation of β -decay effective operators we include just the leading terms of these many-body contributions in the perturbative expansion of the $\hat{\Theta}$ box, namely the second-order two-body diagrams (a) and (b), that are reported in Fig. 1.

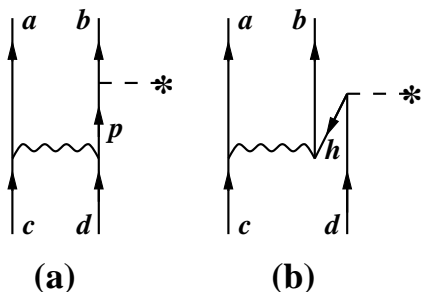


FIG. 1. Second-order two-body diagrams which are included in the perturbative expansion of Θ_{eff} . The dashed line indicates the bare second- and fourth-forbidden β -decay operators Θ , the wavy line the two-body potential $V_{\text{low-}k}$. For the sake of simplicity, for each topology only one of the diagrams which correspond to the permutation of the external lines has been drawn.

The two topologies of second-order connected two-valence-nucleon diagrams (a) and (b) accounts for the so-called “blocking effect”, which is necessary to consider

the Pauli exclusion principle in systems with more than one valence nucleon [50], if the transition operator has a one-body structure. It is worth to point out that these two-body contributions to the effective decay operators mirror the role of induced three-body forces in the calculation of the \hat{Q} box, which we have introduced in section II A.

In the present work, the decay operators Θ are the one-body electric-quadrupole $E2$ transition $q_{p,n} r^2 Y_m^2(\hat{r})$ – the charge $q_{p,n}$ being e for protons and 0 for neutrons –, as well as the one-body second- and fourth-forbidden β -decay operators, as introduced in Sec. II B.

III. RESULTS

In this section we present the results of our SM calculations. First, we compare theoretical and experimental low-energy spectroscopic properties of the parent and daughter nuclei under investigation, namely ^{94}Nb , ^{94}Mo , ^{99}Tc , ^{99}Ru , ^{113}Cd , ^{113}In , ^{115}In and ^{115}Sn . Successively, we focus to study β -decay properties between the ground states (g.s.) of these nuclei.

We point out that, rather than compare the experimental and calculated half-lives, we consider the quantity $\log ft$ to describe the strength of a β -transition. This is defined as the logarithm of

$$ft = \frac{\kappa}{C} \int_1^{w_0} p_e w_e (w_0 - w_e)^2 F(Z, w_e) dw_e . \quad (33)$$

It is worth to stress again that all the calculations have been performed without any empirical renormalization of H_{eff} , as well as without resorting to quenching factors of the axial constant g_A .

A. Spectroscopy

In Table I we compare the low-energy spectra of the nuclei under investigation.

The calculated energy levels are in reasonable agreement with the corresponding experimental states with a few exceptions, while the comparison between theory and experiment for the observed $B(E2)$ (Table II) is less satisfactory for some transitions. In fact, except for the ^{99}Tc , almost all the other calculated $B(E2)$ s underestimate the experimental ones.

Here, it is worth to notice that a sound shell-model description of these nuclei is not an easy task for different reasons, especially in a parameter free calculation. In fact, we start from a ^{78}Ni core, and, therefore, the number of valence particle is sizeable, ranging from 16 to 37. Then, the inclusion of the contributions from three-body diagrams is only the leading order of many-body contributions, whose role grows when increasing the number of valence nucleons. Besides this, Cd, In and Sn isotopes are at the limit of the proton configuration space and, therefore, $Z = 50$ cross-shell excitations

TABLE I. Theoretical versus experimental low-energy levels of the nuclei under investigation.

	J^π	E^{th} (MeV)	E^{Exp} (MeV)
^{94}Nb	6^+	0.000	0.000
	3^+	0.014	0.041
	4^+	0.014	0.058
	7^+	0.017	0.079
^{94}Mo	0^+	0.000	0.000
	2^+	0.836	0.871
	4^+	1.450	1.574
^{99}Tc	9^+	0.000	0.000
	7^+	0.140	0.140
	1^-	0.794	0.143
	5^+	0.812	0.181
	3^+		0.181
^{99}Ru	5^+	0.000	0.000
	3^+	0.343	0.096
	3^+	0.433	0.321
	7^+	0.588	0.341
	3^+		0.341
^{113}Cd	1^+	0.000	0.000
	11^-	0.069	0.263
	3^+	0.019	0.299
	3^+	0.401	0.316
^{113}In	9^+	0.000	0.000
	1^-	1.375	0.392
	3^-	1.613	0.646
	5^+	1.270	1.024
^{115}In	9^+	0.000	0.000
	1^-	1.196	0.336
	3^-	1.445	0.597
	3^+	2.444	0.828
^{115}Sn	1^+	0.068	0.000
	3^+	0.000	0.497
	7^+	0.233	0.612
	$\frac{11}{2}^-$	0.396	0.713

may play a relevant role in the renormalization of the electric-quadrupole transition operator [52, 53]. Actually, the enlargement of the proton model space, in order to account explicitly for such excitations, is out of the present computational resources since the dimensions of the Hamiltonians to be diagonalized could reach $\approx 10^{13}$.

B. Forbidden β decays of ^{94}Nb , ^{99}Tc , ^{113}Cd , and ^{115}In

We focus now on the properties of the β decay between ground states, and it is important to start by discussing the relevance of the CVC relations (See Eq. 28) in determining the *relativistic* form factors.

As shown in Table III, in the case of ^{94}Nb , ^{99}Tc second-forbidden β decays, the *relativistic* form

TABLE II. Theoretical versus experimental [51] low-energy $B(E2)$ transition strengths, in W.u., of the nuclei under investigation.

Nucleus	$J_i \rightarrow J_f$	Theory	Experiment
^{94}Mo	$2^+ \rightarrow 0^+$	7.9	26 (4)
	$4^+ \rightarrow 2^+$	7.7	16.0 (4)
^{99}Tc	$\frac{7}{2}^+ \rightarrow \frac{9}{2}^+$	21	30 (19)
	$\frac{5}{2}^+ \rightarrow \frac{9}{2}^+$	10.3	15.1 (5)
^{99}Ru	$\frac{3}{2}^+ \rightarrow \frac{5}{2}^+$	7.4	50.1 (10)
^{113}Cd	$\frac{3}{2}^+ \rightarrow \frac{1}{2}^+$	2	20 (8)
	$\frac{5}{2}^+ \rightarrow \frac{1}{2}^+$	7.0	0.372 (25)
^{113}In	$\frac{5}{2}^+ \rightarrow \frac{9}{2}^+$	7.2	3.9 (4)
^{115}In	$\frac{1}{2}^+ \rightarrow \frac{3}{2}^+$	17	121 (23)
^{115}Sn	$\frac{3}{2}^+ \rightarrow \frac{1}{2}^+$	0.1	2.1 (6)
	$\frac{7}{2}^+ \rightarrow \frac{3}{2}^+$	0.010	0.130 (4)

factors ${}^V F_{211}$ obtained using the bare operator is zero since the SPMEs of the corresponding operator (Eq. 24) are identically zero in the model space. Even though the renormalization procedure gives SPMEs different from zero, the value of the ${}^V F_{211}$ form factors calculated using the effective operator has an opposite sign, and it is a factor two smaller than the form factor obtained by using the CVC relation (${}^V F_{211}^{CVC}$).

TABLE III. ^{94}Nb , ^{99}Tc , ^{113}Cd , and ^{115}In β decay *relativistic* form factors determined with and without resorting to the CVC relations, and the *non-relativistic* form factors connected with the *relativistic* ones by CVC. The values are in adimensional units.

	Bare	Effective
^{94}Nb		
${}^V F_{211}$	0.000	0.009
${}^V F_{211}^{CVC}$	-0.031	-0.016
${}^V F_{220}$	0.304	0.164
^{99}Tc		
${}^V F_{211}$	0.000	0.008
${}^V F_{211}^{CVC}$	-0.030	-0.017
${}^V F_{220}$	0.286	0.161
^{113}Cd		
${}^V F_{431}$	0.0003	-0.008
${}^V F_{431}^{CVC}$	0.032	0.015
${}^V F_{440}$	-0.521	-0.237
^{115}In		
${}^V F_{431}$	-0.0004	-0.009
${}^V F_{431}^{CVC}$	0.031	0.017
${}^V F_{440}$	-0.473	-0.267

As regards the fourth-forbidden form factors of ^{113}Cd , it is interesting to note that, in this case, the bare value of the *relativistic* form factor ${}^V F_{431}$ has the same sign of ${}^V F_{431}^{CVC}$, but it is two order of magnitude smaller. The

effect of the renormalization is remarkable, but, as it happens for the *relativistic* form factor of the ^{94}Nb , ^{99}Tc decays, the final result again has an opposite sign and is a factor two smaller with respect to the one calculated with the form factor ${}^V F_{431}^{\text{CVC}}$.

The same considerations may be drawn for ^{115}In , except that, using the bare operator, the sign of ${}^V F_{431}$ form factor is not consistent with the one obtained with the ${}^V F_{431}^{\text{CVC}}$ one.

These results point out to a problem in determining the *relativistic* form factors within the non-relativistic reduction of the Dirac equation for the nuclei under investigations. On the above grounds, in the following calculation of the β decay properties we use the CVC relations for the *relativistic* form factors.

TABLE IV. Theoretical and experimental $\log ft$ values. Data are taken from Ref. [51].

	Bare	Effective	Exp.
^{94}Nb	11.30	11.58	11.95 (7)
^{99}Tc	11.580	11.876	12.325 (12)
^{113}Cd	21.902	22.493	23.127 (14)
^{115}In	21.22	21.64	22.53 (3)

We start the discussion of our results from the comparison between our calculated values of the $\log ft$ s and the experimental ones, as they are reported in Table IV. There, we have reported the $\log ft$ s obtained using both the bare second- and fourth-forbidden β -decay operators and the effective ones. It is worth stressing again that, as we have reported in Sec. II C, our SM effective operators consists of one- and two-body components.

As can be seen, the results that are obtained by employing the bare β -decay operators underestimate the experimental $\log ft$ s, a result that is consistent with the general consideration that nuclear models, which operate truncation of the Hilbert space of the single-nucleon configurations, require the introduction of a quenching factor q in order to reproduce the experimental half-lives for allowed β -decay transitions (see for example Refs. [1, 2]).

On the other hand, the calculations employing the SM effective operators provide results that substantially recover the gap with respect to the experimental $\log ft$ s, a result that is consistent with our previous studies of the allowed β -decay within the realistic shell model [7–10].

In order to discuss the role of the renormalization of the β -decay operator on the calculation of the shape of forbidden β -decay energy spectra, we evaluate the quenching factors that are needed to tune the axial coupling constant g_A in order to obtain the same results we have obtained for the $\log ft$ s by employing the SM effective operators. Using Eq. (7), we obtain that the quenching factors that reproduce the values in column “Effective” in Table IV are $q = 0.27, 0.50, 0.22,$ and 0.41 for ^{94}Nb , ^{99}Tc , ^{113}Cd , and ^{115}In decays, respectively.

In Fig. 2, the calculated and experimental normalized

spectra of the second-forbidden and fourth-forbidden decays, that are under our present investigation, are reported. The available data are drawn, with the corresponding errors, using red dots. It should be noted that the energy spectra are normalized in the energy region of the available data, and that those for ^{99}Tc decay have been extracted from Fig. (5) in Ref. [42]. Moreover, the experimental spectra of ^{99}Tc and ^{113}Cd are obtained after an unfolding procedure which takes into account the detector response function, as discussed in Ref. [54] and Refs. [42, 55], respectively. Conversely, in the energy spectrum of ^{115}In the detector response is not decoupled, leading to a more difficult direct comparison. However, according to the results presented in Refs. [20, 56], the detector response effects are expected to be small and, in any case, not significant for our purposes.

As regards ^{94}Nb decay, there are no experimental results, at present, and they are normalized in the full range of the kinetic-energy interval.

The calculated values are labelled and drawn as follows:

- (I) the calculated values, obtained using the bare operators, follow the dashed blue line;
- (II) the spectra calculated using the SM effective operators are drawn with a continuous black line;
- (III) finally, we report also the results coming out by using the bare operator, but quenching the axial coupling constant g_A with the q factors that reproduce the theoretical $\log ft$ s using the effective decay operators.

From the inspection of Fig. 2, we can clearly assert that the theoretical energy spectra, calculated employing the bare and the effective β -decay operators, are in a very good agreement with the corresponding experimental shapes [20, 42, 54, 57], for the forbidden β -decays of ^{99}Tc , ^{113}Cd , and ^{115}In . Moreover, all of them exhibit a small sensitivity to the renormalization of the β -decay operators, with small differences appearing only at low energy for all the decays ($\lesssim 100$ keV).

As regards the energy spectra obtained with the bare operator and quenching g_A , we see that they show a pronounced disagreement with the experimental shapes, for ^{99}Tc , ^{113}Cd , and ^{115}In , mostly in the low- and intermediate-energy intervals.

These results lead us to two main conclusions.

First, the calculated shapes of the normalized energy spectra are substantially insensitive to the renormalization of the forbidden β -decay operator by way of many-body perturbation theory, that is our approach to realistic shell model, and are in a good agreement with current data.

Second, it seems that the mere renormalization of the axial coupling constant g_A by a quenching factor q makes it difficult to provide simultaneously better $\log ft$ s and shapes of the energy spectra which reproduce the observed behavior.

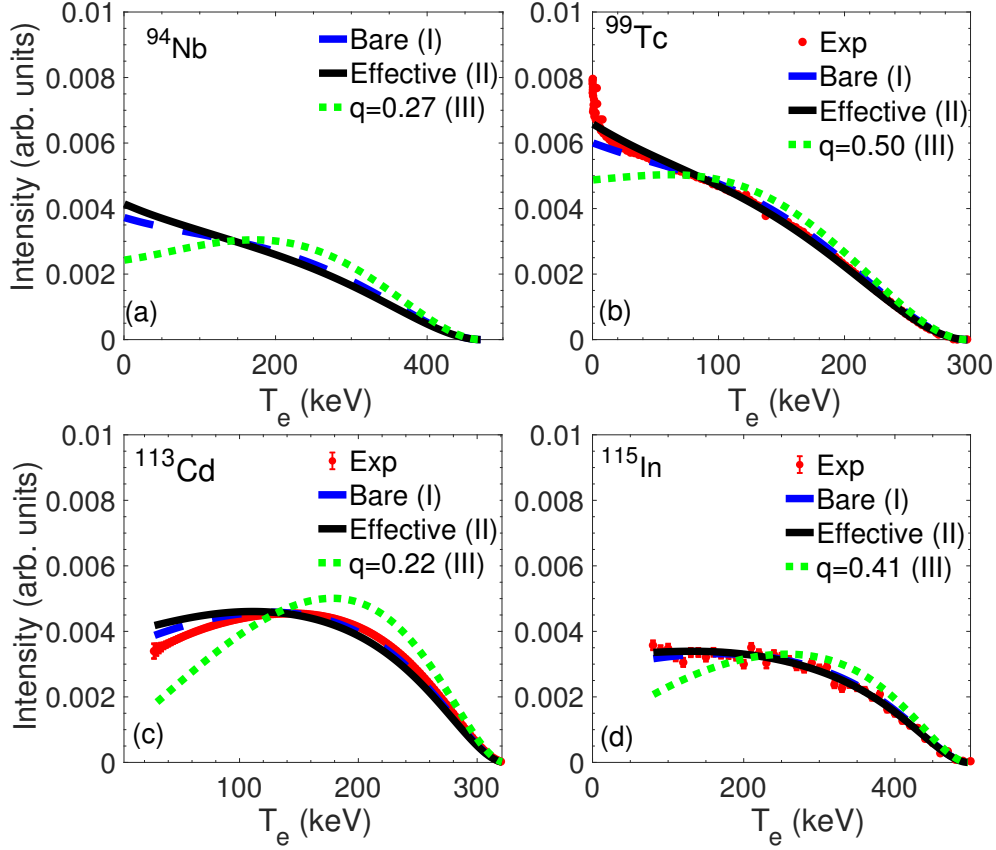


FIG. 2. Theoretical and experimental normalized β -spectra of ^{94}Nb (a), ^{99}Tc (b), ^{113}Cd (c) and ^{115}In (d) as a function of the electron kinetic energy T_e . The theoretical spectra are calculated with the bare operator (blue dashed line), the SM effective operator (continuous black line), and using the quenching factors for g_A extracted from Eq. (34) (green dashed line) (see text for details). The red dots corresponds to experimental values, where they are available [20, 42, 54, 57].

It is worth mentioning that in Refs. [13, 42, 58] the authors carried out a study of the sensitivity of their calculated spectra upon the renormalization of the axial coupling constant, and they found a noticeable dependence of their results on the choice of the quenching factor q .

Now, in order to reach a better insight of the results, we analyze the different components of the shape factor defined in Eq. (7). This factor can be divided in three components, the vector, axial and vector-axial terms, namely

$$C(w_e) = C_V(w_e) + C_A(w_e) + C_{VA}(w_e), \quad (34)$$

where C_V contains the coupling constant g_V^2 , C_A contains g_A^2 and C_{VA} contains $g_V \cdot g_A$.

The integrated shape functions \tilde{C}_k are reported in Table V, as well as the total value \tilde{C} (see Eq.(7)) for all the decays under investigation. As can be seen, at variance with what was observed in Ref. [14], for all the decays \tilde{C}_{VA} is positive and therefore it is summed in phase with the vector and axial components.

Actually, such a result is a consequence of the CVC theory, since if we do not use the CVC relations to determine the *relativistic* form factor, the mixed terms \tilde{C}_{VA} for the cases under investigation become negative, and

very close in absolute value to the sum of the correspondent vector and axial components. This is similar to the results reported in Ref. [14], and such a feature highlights the relevance of this form factor, as it was also discussed in other papers [35, 37, 40–42].

Even though it is small compared to the other form factors, the *relativistic* one is relevant to determine $C(w_e)$, and, therefore, shapes and half-lives, since, at variance with *non-relativistic* form factors, it enters the quantity $M_K(k_e, k_\nu)$ of Eq. (9) without any suppression coefficient (for the explicit expression of $M_K(k_e, k_\nu)$ see Table 4 in Ref. [34]).

The positive values of \tilde{C}_{VA} explain the stability of the shape with respect to the renormalization of the decay operators. In fact, without using the CVC relations, as a consequence of the delicate balance of the vector, axial and vector-axial terms, it is obtained a shape of the energy spectrum that is very sensitive to the renormalization procedure.

TABLE V. Integrated shape functions \tilde{C} of the studied transitions and their vector \tilde{C}_V , axial-vector \tilde{C}_A , and mixed components \tilde{C}_{VA} .

Parent	Op	\tilde{C}_V	\tilde{C}_A	\tilde{C}_{VA}	\tilde{C}
^{94}Nb	Bare	5.44×10^{-9}	1.23×10^{-8}	1.34×10^{-8}	3.11×10^{-8}
	Effective	1.40×10^{-9}	9.07×10^{-9}	5.72×10^{-9}	1.62×10^{-8}
^{99}Tc	Bare	3.10×10^{-9}	5.90×10^{-9}	7.15×10^{-9}	1.61×10^{-8}
	Effective	8.82×10^{-10}	4.14×10^{-9}	3.14×10^{-9}	8.17×10^{-9}
^{113}Cd	Bare	1.19×10^{-19}	3.72×10^{-19}	2.80×10^{-19}	7.70×10^{-19}
	Effective	2.14×10^{-20}	1.14×10^{-19}	6.20×10^{-20}	1.98×10^{-19}
^{115}In	Bare	6.14×10^{-19}	1.93×10^{-18}	1.15×10^{-18}	3.69×10^{-18}
	Effective	1.75×10^{-19}	8.68×10^{-19}	3.72×10^{-19}	1.42×10^{-18}

IV. CONCLUSIONS AND OUTLOOK

This work is the first attempt to describe the features of forbidden β -decays within the framework of the realistic shell model, without resorting to any phenomenological quenching factor for the axial and vector coupling constants.

Such a study represents not only a validation of our theoretical framework to assess the reliability to predict $0\nu\beta\beta$ nuclear matrix elements [11], but can give also useful information for the recent experimental studies of the electron energy spectra of forbidden β -decays.

First, we have verified the ability of our effective Hamiltonian and transition operators by comparing the calculated low-energy spectra and $E2$ transition strengths of parent and daughter nuclei, involved in the forbidden β -decays under consideration, with their experimental counterparts. The comparison of the spectroscopic data with the corresponding experimental ones is quite satisfactory, especially if we consider the large number of valence particles – ranging from 16 to 37 –, which characterizes the nuclear system we have investigated.

Then, we have calculated both the half-lives and the energy spectra of the emitted electrons of the second-forbidden β -decay of ^{94}Nb and ^{99}Tc , and the fourth-forbidden β -decay of ^{113}Cd and ^{115}In .

As regards the outcome of our calculation of the properties of the forbidden β -decay processes under investigation, the results may be outlined as follows:

- The exam of the theoretical $\log ft_s$ and the experimental ones shows that the results that are obtained with bare operators always underestimate the data, a feature that is resembling the problem of the quenching of g_A in the allowed β -decay transitions. The theory moves towards experiment by employing the theoretical effective operators, as expected.
- Starting from the wave functions that are obtained through the diagonalization of our H_{eff} , the shape of the calculated energy spectra is rather insensitive to the choice of the β -decay operator, bare or

effective, and in both cases the reproduction of the observed normalized energy spectra is more than satisfactory.

- The latter result seems to be unrelated to the considerations about the calculated $\log ft_s$, and the comparison with data. In fact, using the bare operator, but introducing a quenching factor of the axial constant to improve the reproduction of the experimental $\log ft_s$, it results in a distortion of the shape of the energy spectra, that affects the agreement with the observed ones.

Wrapping up the results we have obtained, we may say that the goal to obtain, on the same footing, a better reproduction of half-lives and the shape of the energy spectrum of the emitted electrons in forbidden β decays, by employing effective decay operators, is a delicate matter. As it has been mentioned in Sec. III B, such an issue was met also in other studies [13, 42, 58], where the authors showed that, without a renormalization of the β -decay operator that is framed in the many-body theory, the reproduction of the observed properties of forbidden β decays cannot rely only on the quenching of g_A , and other empirical parameters should be considered.

It is worth pointing out that such an issue does not emerge in the study of allowed β decays, since the calculated energy spectrum does not depend on the nuclear matrix element of the electroweak currents, and the most relevant observable to be tested is the half-life.

Our considerations lead to suggest that the study of forbidden β -decay processes could be a valuable tool to refine the theoretical knowledge of the renormalization of transition operators, and to rule out models that could be not reliable to predict the value of nuclear matrix elements for decays, such as in the case of the $0\nu\beta\beta$ decay.

On the above grounds, we plan to extend the present work by studying forbidden β decays in other mass regions, close to nuclei that are candidates for detecting the $0\nu\beta\beta$ decay. Another interesting subject could be to tackle the forbidden β -decay problem starting from the derivation of electroweak currents by way of the chiral perturbation theory, which represent the new frontier to

frame the nuclear many-body problem within its underlying fundamental theory – the QCD –, and it is currently employed to investigate GT transitions with different nuclear approaches [10, 59–64].

V. ACKNOWLEDGMENTS

We thank J. Kostensalo, T. Miyagi, M. Biassoni, C. Brofferio, S. Ghislandi, A. Nava and L. Pagnanini for useful comments and discussion. G. D. G. acknowledges the support from the EU-FESR, PON Ricerca e Innovazione 2014-2020 - DM 1062/2021. We acknowledge the CINECA award under the ISCRA initiative and under the INFN-CINECA agreement, for the availability of high performance computing resources and support. This work is partly supported by the Czech Science Foundation (Czech Republic) P203-23-06439S.

-
- [1] G. Martínez-Pinedo, A. Poves, E. Caurier, and A. P. Zuker, *Phys. Rev. C* **53**, R2602 (1996).
- [2] J. Barea, J. Kotila, and F. Iachello, *Phys. Rev. C* **91**, 034304 (2015).
- [3] J. Suhonen and J. Kostensalo, *Frontiers in Physics* **7**, 29 (2019).
- [4] T. T. S. Kuo and E. Osnes, *Lecture Notes in Physics*, vol. 364 (Springer-Verlag, Berlin, 1990).
- [5] K. Suzuki and R. Okamoto, *Prog. Theor. Phys.* **93**, 905 (1995).
- [6] L. Coraggio and N. Itaco, *Frontiers in Physics* **8**, 345 (2020).
- [7] L. Coraggio, L. De Angelis, T. Fukui, A. Gargano, and N. Itaco, *Phys. Rev. C* **95**, 064324 (2017).
- [8] L. Coraggio, L. De Angelis, T. Fukui, A. Gargano, N. Itaco, and F. Nowacki, *Phys. Rev. C* **100**, 014316 (2019).
- [9] L. Coraggio, N. Itaco, G. De Gregorio, A. Gargano, R. Mancino, and F. Nowacki, *Phys. Rev. C* **105**, 034312 (2022).
- [10] L. Coraggio, N. Itaco, G. De Gregorio, A. Gargano, Z. H. Cheng, Y. Z. Ma, F. R. Xu, and M. Viviani, *Phys. Rev. C* **109**, 014301 (2024).
- [11] L. Coraggio, A. Gargano, N. Itaco, R. Mancino, and F. Nowacki, *Phys. Rev. C* **101**, 044315 (2020).
- [12] M. T. Mustonen, M. Aunola, and J. Suhonen, *Phys. Rev. C* **73**, 054301 (2006).
- [13] M. Haaranen, P. C. Srivastava, and J. Suhonen, *Phys. Rev. C* **93**, 034308 (2016).
- [14] M. Haaranen, J. Kotila, and J. Suhonen, *Phys. Rev. C* **95**, 024327 (2017).
- [15] J. Kostensalo, J. Suhonen, J. Volkmer, S. Zatschler, and K. Zuber, *Phys. Lett. B* **822**, 136652 (2021).
- [16] J. Kostensalo, E. Lisi, A. Marrone, and J. Suhonen, *Phys. Rev. C* **107**, 055502 (2023).
- [17] K. Zuber, *Physics Letters B* **519**, 1 (2001).
- [18] C. Goessling, M. Junker, H. Kiel, D. Muenstermann, S. Oehl, and K. Zuber, *Phys. Rev. C* **72**, 064328 (2005).
- [19] L. Bodenstern-Dresler, Y. Chu, D. Gehre, C. Gößling, A. Heimbold, C. Herrmann, R. Hodak, J. Kostensalo, K. Kröniger, J. Küttler, et al., *Physics Letters B* **800**, 135092 (2020).
- [20] L. Pagnanini, G. Benato, P. Carniti, E. Celi, D. Chiesa, J. Corbett, I. Dafinei, S. Di Domizio, P. Di Stefano, S. Ghislandi, et al., *The European Physical Journal Plus* **138**, 445 (2023).
- [21] M. Biassoni, C. Brofferio, S. Capelli, F. Cappuzzello, M. Carminati, M. Cavallaro, L. Coraggio, O. Cremonesi, G. De Gregorio, C. Fiorini, et al., *J. Phys. Conf. Ser.* **2453**, 012020 (2023).
- [22] R. Machleidt, *Phys. Rev. C* **63**, 024001 (2001).
- [23] S. Bogner, T. T. S. Kuo, L. Coraggio, A. Covello, and N. Itaco, *Phys. Rev. C* **65**, 051301(R) (2002).
- [24] L. Coraggio, A. Covello, A. Gargano, N. Itaco, and T. T. S. Kuo, *Prog. Part. Nucl. Phys.* **62**, 135 (2009).
- [25] M. Hjorth-Jensen, T. T. S. Kuo, and E. Osnes, *Phys. Rep.* **261**, 125 (1995).
- [26] L. Coraggio, A. Covello, A. Gargano, N. Itaco, and T. T. S. Kuo, *Ann. Phys. (NY)* **327**, 2125 (2012).
- [27] L. Coraggio, L. De Angelis, T. Fukui, A. Gargano, and N. Itaco, *J. Phys. Conf. Ser.* **1056**, 012012 (2018).
- [28] E. M. Krenciglowa and T. T. S. Kuo, *Nucl. Phys. A* **235**, 171 (1974).
- [29] K. Suzuki and S. Y. Lee, *Prog. Theor. Phys.* **64**, 2091 (1980).
- [30] K. Suzuki, R. Okamoto, H. Kumagai, and S. Fujii, *Phys. Rev. C* **83**, 024304 (2011).
- [31] N. Shimizu, T. Mizusaki, Y. Utsuno, and Y. Tsunoda, *Computer Physics Communications* **244**, 372 (2019).
- [32] L. Coraggio, G. De Gregorio, A. Gargano, N. Itaco, T. Fukui, Y. Z. Ma, and F. R. Xu, *Phys. Rev. C* **102**, 054326 (2020).
- [33] See Supplemental Material at [URL will be inserted by publisher] for the list of single-particle energies and two-body matrix elements of the shell-model Hamiltonian H_{eff} , derived for 20 and 15 valence protons and neutrons, respectively, namely for ^{113}Cd .
- [34] H. Behrens and W. Bühring, *Nucl. Phys. A* **162**, 111 (1971).
- [35] D. Fahlín Strömberg, Ph.D. thesis (2020), URL <https://tuprints.ulb.tu-darmstadt.de/13302>.
- [36] J. C. Hardy and I. S. Towner, *Phys. Rev. C* **79**, 055502 (2009).
- [37] R. Sadler and H. Behrens, *Zeitschrift für Physik A Hadrons and Nuclei* **346**, 25 (1993).
- [38] Q. Zhi, E. Caurier, J. J. Cuenca-García, K. Langanke, G. Martínez-Pinedo, and K. Sieja, *Phys. Rev. C* **87**, 025803 (2013).
- [39] M. E. Rose and R. K. Osborn, *Phys. Rev.* **93**, 1326 (1954).
- [40] O. S. Kirsebom, M. Hukkanen, A. Kankainen, W. H. Trzaska, D. F. Strömberg, G. Martínez-Pinedo, K. An-

- dersen, E. Bodewits, B. A. Brown, L. Canete, et al., *Phys. Rev. C* **100**, 065805 (2019).
- [41] K. Kossert, M. Loidl, X. Mougeot, M. Paulsen, P. Ranitzsch, and M. Rodrigues, *Applied Radiation and Isotopes* **185**, 110237 (2022).
- [42] M. Paulsen, P. Ranitzsch, M. Loidl, M. Rodrigues, K. Kossert, X. Mougeot, A. Singh, S. Leblond, J. Beyer, L. Bockhorn, et al., *arXiv* (2023), 2309.14014.
- [43] H. A. Smith and P. C. Simms, *Phys. Rev. C* **1**, 1809 (1970).
- [44] M. Antony, A. Pape, and J. Britz, *Atomic Data and Nuclear Data Tables* **66**, 1 (1997).
- [45] H. A. Mavromatis, L. Zamick, and G. E. Brown, *Nucl. Phys. A* **80**, 545 (1966).
- [46] H. A. Mavromatis and L. Zamick, *Nucl. Phys. A* **104**, 17 (1967).
- [47] P. Federman and L. Zamick, *Phys. Rev.* **177**, 1534 (1969).
- [48] P. J. Ellis and E. Osnes, *Rev. Mod. Phys.* **49**, 777 (1977).
- [49] I. S. Towner and K. F. C. Khanna, *Nucl. Phys. A* **399**, 334 (1983).
- [50] I. S. Towner, *Phys. Rep.* **155**, 263 (1987).
- [51] Data extracted using the NNDC On-line Data Service from the ENSDF database., URL <https://www.nndc.bnl.gov/ensdf>.
- [52] L. Coraggio, A. Covello, A. Gargano, N. Itaco, and T. T. S. Kuo, *Phys. Rev. C* **91**, 041301 (2015).
- [53] L. Coraggio, A. Gargano, and N. Itaco, *Phys. Rev. C* **93**, 064328 (2016).
- [54] P. Belli, R. Bernabei, N. Bukilic, F. Cappella, R. Cerulli, C. J. Dai, F. A. Danevich, J. R. d. Laeter, A. Incicchitti, V. V. Kobychchev, et al., *Phys. Rev. C* **76**, 064603 (2007).
- [55] M. Paulsen, K. Kossert, and J. Beyer, *Nuclear Instruments and Methods in Physics Research Section A: Accelerators, Spectrometers, Detectors and Associated Equipment* **953**, 163128 (2020).
- [56] L. Pagnanini, G. Benato, P. Carniti, E. Celi, D. Chiesa, J. Corbett, I. Dafinei, S. D. Domizio, P. D. Stefano, S. Ghislandi, et al., *arXiv* (2024), 2401.16059.
- [57] P. Belli, R. Bernabei, F. A. Danevich, A. Incicchitti, and Tretyak, *Eur. Phys. J. A* **55**, 140 (2019).
- [58] J. Kostensalo and J. Suhonen, *Phys. Rev. C* **96**, 024317 (2017).
- [59] P. Gysbers, G. Hagen, J. D. Holt, G. R. Jansen, T. D. Morris, P. Navrátil, T. Papenbrock, S. Quaglioni, A. Schwenk, S. R. Stroberg, et al., *Nature Phys.* **15**, 428 (2019).
- [60] G. B. King, L. Andreoli, S. Pastore, M. Piarulli, R. Schiavilla, R. B. Wiringa, J. Carlson, and S. Gandolfi, *Phys. Rev. C* **102**, 025501 (2020).
- [61] A. Baroni, G. B. King, and S. Pastore, *Few-Body Syst.* **62**, 114 (2021).
- [62] A. Gnech, L. E. Marcucci, R. Schiavilla, and M. Viviani, *Phys. Rev. C* **104**, 035501 (2021).
- [63] A. Gnech and R. Schiavilla, *Phys. Rev. C* **106**, 044001 (2022).
- [64] G. B. King, A. Baroni, V. Cirigliano, S. Gandolfi, L. Hayen, E. Mereghetti, S. Pastore, and M. Piarulli, *Phys. Rev. C* **107**, 015503 (2023).